Improved Sea Surface Height from Satellite Altimetry in Coastal Zones: A Case Study in Southern Patagonia

L.S. Lago, M. Saraceno, L.A. Ruiz Etcheverry, M. Passaro, F. Oreiro, E.E. D'Onofrio, R. A. González

***Abstract*- High resolution 20-Hz Jason-2 satellite altimetry data obtained from crossing tracks numbered 52 and 189 in San Matias Gulf, Argentina, are compared with a 22-month-longtime series of sea level measured by a bottom pressure recorder. It was deployed 1.3km from the nominal intersection of the two tracks and 0.9km from the coast. Results show that by improving retracking and tidal modeling, satellite altimetry data become more accurate close to the coast. Indeed, a larger number of reliable data are obtained up to 1.6km from the coast when satellite data are retracked using ALES (Adaptive Leading Edge Subwaveform retracker) rather than using the classic Brown model. The tidal model that showed the lowest root sum square of the difference (*RSS*) between the in situ and the modelled tidal amplitude and phase is TPXO8 (*RSS* 4.8cm). Yet, the lowest difference from in situ tidal constituents is obtained by harmonic analysis of the available 23-year-long 1-Hz altimetry data set (*RSS* 4.1cm), highlighting the potential of altimetry data to compute tides. Considering ALES retracking and TPXO8 tidal correction for the 20-Hz Jason-2 data, we finally show that it is possible to retrieve 70% more data and to improve correlation with in situ measurements from 0.79 to 0.95. The sea level anomaly obtained this way has a root mean square difference (*RMSD*) from in situ data of only 13cm as close as 4km from the coast. Overall, the analysis performed indicates satellite altimetry data can be greatly improved, even in complex macrotidal coastal regions.**

***Index Terms*- Along-track, bottom pressure recorder, coastal altimetry, Jason-2, macrotidal regime, San Matias Gulf, satellite altimetry accuracy, sea level anomaly, Patagonia Argentine**

L.S. Lago is with the Departamento de Ciencias de la Atmósfera y los Océanos (DCAO), Ciudad Autónoma de Buenos Aires, C1428EGA, Argentina (e-mail: loreleylago@gmail.com).

M. Saraceno is with the Departamento de Ciencias de la Atmósfera y los Océanos (DCAO), Ciudad Autónoma de Buenos Aires, C1428EGA, Argentina; the Centro de Investigación del Mar y la Atmósfera (CIMA), Ciudad Autónoma de Buenos Aires, C1428EGA, Argentina; and the UMI-IFAECI (e-mail: saraceno@cima.fcen.uba.ar).

L.A. Ruiz Etcheverry is with the International Pacific Research Center, School of Ocean and Earth Science and Technology, University of Hawaii, Honolulu, Hawaii, USA (e-mail: laurare@hawaii.edu).

M. Passaro is with the Deutsches Geodätisches Forschungsinstitut der Technischen Universität München, Arcistrasse 21, 80333, München, Germany (e-mail: marcello.passaro@tum.de).

F. Oreiro and E.E. D'Onofrio are with the Departamento de Oceanografía, Servicio de Hidrografía Naval (SHN), Ciudad Autónoma de Buenos Aires, C1270ABV, Argentina and the Facultad de Ingeniería, Universidad de Buenos Aires, Ciudad Autónoma de Buenos Aires, C1127AAR, Argentina (e-mails: feroreiro@yahoo.com.ar;eedonofrio@yahoo.com.ar).

R. A. González is with CONICET - Escuela Superior de Ciencias Marinas / Instituto de Biología Marina y Pesquera Almirante Storni (Universidad Nacional del Comahue), Río Negro, Argentina (e-mail: racg05@gmail.com).

NOMENCLATURE

ALES	Adaptive Leading Edge Subwaveform.
AVISO	Archiving, Validation and Interpretation of Oceanographic Data.
BPR	Bottom pressure recorder.
C	Conductivity.
CL	Confidence level.
CLS	Collect Localisation Satellites.
CNES	Centre National d'Études Spatiales.
CTOH	Centre of Topography of the Oceans and the Hydrosphere.
DAC	Dynamic Atmospheric Correction.
f_j	Nodal factor.
g	Gravity of the j tidal constituent.
g_j	Epoch of the j tidal constituent.
$h(t)$	Height of the tide at observation time t.
H	Tidal amplitude.
IOC	Intergovernmental Oceanographic Commission.
j	Tidal constituent.
J1	Jason-1.
J2	Jason-2.
MSS	Mean sea surface.
n	Number of tidal constituents considered to calculate *RSS*.
NCEP	National Center for Environmental Prediction.
P_{abs}	Pressure measured by BPR.
P_{atm}	Atmospheric pressure.
PCS	Patagonian Continental Shelf.
RMSD	Root mean square difference.
RMS	Root mean square.
RMS_{misfit}	Root mean square misfit,= $\sqrt{\frac{(H_1 cos(\phi_1) - H_2 cos(\phi_2))^2 + (H_1 sin(\phi_1) - H_2 sin(\phi_2))^2}{2}}$.
RSS	Root sum square, $= \sqrt{\frac{\sum_{j=1}^{n} RMS_{misfit_j}^{\ 2}}{n}}$.
S	Salinity.
S-GDR	Sensor Geophysical Data Records.
SHN	Servicio de Hidrografía Naval.
SLA	Sea level anomaly.
SLP	Sea level pressure.
SMG	San Matias Gulf.
SSH	Sea surface height, $= \frac{1}{\rho g}(P_{abs} - P_{atm})$.
SST	Sea surface temperature.
t	Time.
T	Temperature.
TG	Tide gauge.
T/P	TOPEX/Poseidon.
V	Angular velocity.
$(V+u)_j$	Equilibrium argument of the j tidal constituent.
Z_0	Mean height of the water level at the beginning of the series.
ΔZ	Linear trend of the series.
ρ	Density.
ϕ	Tidal phase.

I. Introduction

SINCE SPACE agencies managed to control the orbit of the satellites with sufficient accuracy (defined as the degree of closeness of the observation to some universally accepted reference standard [44]), satellite altimetry measurements have become an essential dataset to understand ocean dynamics, monitor climate change and improve forecasts and real-time products through assimilation in operational ocean models, among others. Thus, satellite altimetry data applications have proved to be of great benefit to our society. Yet, the time and spatial sampling of the altimeters are limiting factors for the spatiotemporal resolution of the phenomena we can describe in the ocean. Near the coast, oceanic processes have shorter space and time scales than in the open ocean and thus standard satellite altimetry products are less useful there. Furthermore, altimetry encounters a number of problems over shallow shelves and in the proximity of coasts, where distortions of the altimetric waveforms, non-linear tidal currents and inaccurate atmospheric water vapor corrections are significant factors [47].

It is therefore crucial to assess to what extent satellite altimetry data are reliable close to the coast. In recent years, altimetry data have been successfully used to analyze the sea level variability on seasonal time scales in several coastal regions and shelves around the world [33], [27], [20], [42]. In the Patagonia Continental Shelf (PCS, Fig. 1) the Root Mean Square Differences (*RMSD*) between gridded satellite sea level anomaly (*SLA*) and tide gauge (TG) is lower than 2.1cm on seasonal scales [33]. In [35] it is shown that using gridded altimetry data near the coast of Uruguay and South of Brazil it is possible to identify the expected patterns in SLA, in response to seasonal winds. In the same region, using along-track data, [42] found no evidence that errors in tidal models affect the seasonal sea level variability estimations from satellite altimetry.

To analyze altimetry data close to the coast and at shorter-than-seasonal temporal scales, two aspects are critical: (i) the use of an accurate tidal model and (ii) a retracking algorithm adapted to retrieve sea surface height (*SSH*) close to the coast, e.g. [17]. These two aspects are discussed with more detail below.

A. Retracking

To better understand the retracking process, it is helpful to recall the basics of radar altimetry. The pulse sent by the satellite radar interacts with the sea surface and part of the incident signal is reflected back to the satellite. Then, the received echo pulse is registered on-board in a time series, i.e. a waveform whose leading edge contains the information needed to retrieve the range (the distance between the satellite and the sea surface). In the open ocean, waveforms are characterized by a steep leading edge representing returns coming from scatterers inside the circular footprint, of the specular reflection zone at nadir. The rising time of the leading edge is thus related to the sea state. Once the leading edge has reached its peak, a slowly-decaying trailing edge follows, that represents the returns of off-nadir scatterers. The retracking procedure is based on statistical techniques that consist in fitting the waveform to a functional form [14]. The standard open ocean retracking technique is based on the Brown functional form [4]. The noise in the radar signal can generate inaccuracies in the retrieval of certain parameters, such as the range. In coastal areas, backscattering inhomogeneities of the satellite footprint, which can be due to land or patches of calm water (caused for example by wind sheltering, fronts, natural slicks), are seen as bright targets in the trailing edge of the waveform, whose shape no longer conforms to that assumed by the Brown algorithm. To overcome this difficulty, several "ground-based" retracking procedures have been developed for coastal regions. Thus, retracking allows more accurate data to be extracted near the coastal regions, where data are usually flagged as unreliable in 1Hz altimetry products [10]. The retracking method considered for this paper, the Adaptive Leading Edge Subwaveform (ALES), is a method that has been successfully validated in the Adriatic Sea and in the Greater Agulhas System for satellite missions Envisat, Jason-1 (J1) and Jason-2 (J2) [26]. Retracking data selected for this article was provided by AVISO and is freely available at: ftp://podaac.jpl.nasa.gov/allData/coastal_alt/L2/ALES/.

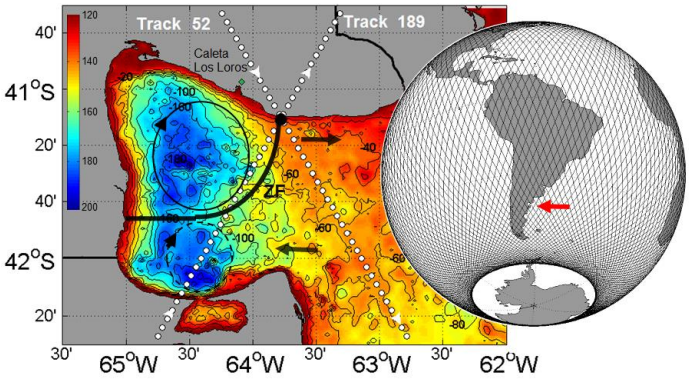

Fig. 1. San Matias Gulf bathymetry (m). White points represent the analyzed J2 satellite tracks, descending track 52 and ascending track 189. The black dot indicates the mooring position with coordinates (41°10.8'S, 63°46.8'W). The intersection between the satellite tracks is located 900m from the coast. Arrows indicate the mean surface circulation adapted from [45]. The surface Zonal Front (ZF) position is represented by the black line. The green diamond is the location of the park ranger's house.

B. Tide Model Comparison

The importance of a tidal model lies in the accurate removal of the tidal signal from the sea level estimated by the altimeter. Clearly the impact of an accurate tidal model is larger in regions characterized by a macrotidal regime, as shown in [34] in the PCS. Causes of the poor performance of the tidal models in coastal regions are that tides become more dependent on bathymetry and the coastline geometry, among other factors. Therefore, a poor knowledge of the bathymetry greatly affects the performance of tidal models.

Nevertheless, depending on the region considered, global tidal models are accurate enough to correct altimetry data even near the coasts [41]. In several macrotidal regions, like San Matias Gulf (SMG), regional models have shown better results than global ones, e.g. [5], [34], [43]. [5] showed that when the appropriate tidal model is used, low-frequency sea level and geostrophic current variations can be reliably observed in altimetry data close to the coast. More examples of the improvements in coastal altimetry data obtained due to the choice of a proper tidal model can be found in [48].

C. Objectives

The objective of the current work is to validate satellite altimetry data in a highly dynamic region dominanted by a macrotidal regime: the SMG in Southern Patagonia, Argentina. Moreover, we aim at describing how close to the coast the altimetric data set is reliable. To achieve this objective, we analyze the performance of the retracking method and of the satellite corrections that must be applied to the radar measurements, focusing on the ocean tidal correction. As a case study, we work in a particular position where a crossover of J2 tracks occurs about 900m from the coast (Fig. 2) and where a bottom pressure recorder (BPR) was moored for 22 months. The intersection of satellite tracks is extremely helpful because it allows the extraction of data at higher temporal resolution than from points along a single track, and from two different overpass directions (enabling vector quantities, such as slope, to be estimated).

D. Paper Organization

The paper is structured as follows. In Section II the study area is described. Section III is dedicated to the description of all databases considered and to the methodologies applied. Results are presented in sections IV and the main conclusions are summarised in Section V.

II. San Matias Gulf

SMG is connected to the Atlantic Ocean through a 100km-long mouth (Fig. 1). Its interior presents a maximum depth of 200m. In addition, there is intense fishing activity, with hake being the principal fishing resource [15]. This is a highly dynamic region characterized by a strong semi-diurnal tidal regime whose range that exceeds 4m. The amplitude of the largest tidal constituent of 2.6m corresponds to the semi-diurnal lunar constituent M_2.

Circulation models [2] provide knowledge of the surface circulation of SMG, which is characterized by two gyres, one in the northern and the other in the southern region of the Gulf (Fig. 1). The intensity of the gyres, caused by westerly winds and tides, varies seasonally [45].

Previous studies of surface salinity from in situ observations [28] show that SMG waters are saltier than those from the adjacent ocean due to an excess in annual evaporation, and also

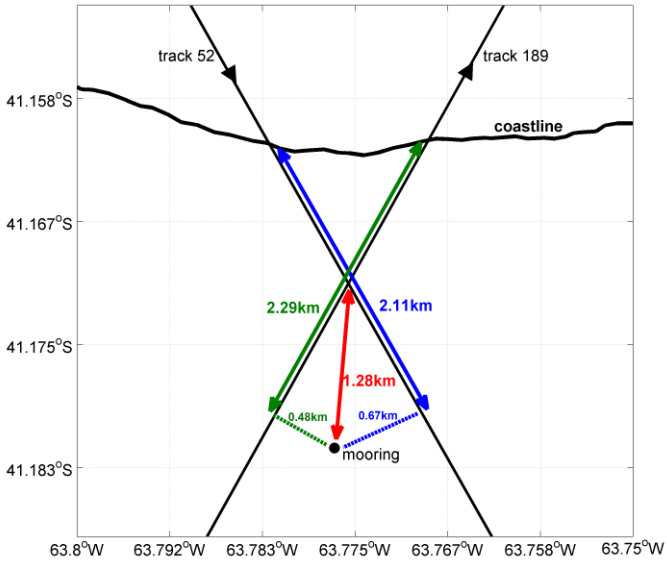

Fig. 2. Zoom of SMG around the mooring position (black dot). The satellite tracks considered are shown (black lines) with arrows that indicate flight direction of the satellite. The distance from the mooring to the coast along track 52 and 189 are indicated in green and blue, respectively. Dashed lines indicate the minimum distance from the mooring to each track. The red line indicates the distance between the mooring position and the satellite track intersection.

suggest that export of waters in the surface occurs mainly in the northern region of the gulf.

Both observations of sea surface temperature (SST) from historical data [8] and model simulations [45] suggest that SMG can be divided into two regions separated by a thermohaline front that remains present most of the year (Fig. 1), except during the winter season. The northern section is warmer than the southern one [49]. This *SST* pattern is coherent with the circulation mentioned earlier; the intrusion of colder water from the PCS into the Gulf happens mainly in the southern region of SMG.

The availability of accurate high-resolution coastline location data plays a key role in interpreting the effect of land on the altimeter signal and in particular, understanding how waveform shapes respond to land in the footprint [14]. In the region of study a cliff about 40m high is present. This cliff is made of soft rock (sand, rocks and soft soil). In such case, the standard definition of coastline is assumed to be the foot of the cliff, e.g. [31]. However, for coastal altimetry purposes, it is more relevant to know the position of the lowest tide. In order to establish its edge, we carefuly analyzed available Landsat images, considering the time at which the image was adquired and the corresponding tidal level. In this way, we established the edge represented in Fig. 2, which is on average 300m seaward at the foot of the cliff. Visual observations from locals correspond very well with our estimation. The shortest distance between the nominal intersection of J2 tracks 189 and 52 and the lowest tide edge estimated is 400m (Fig. 2).

III. DATA

A. In situ Data

The validation of satellite altimetry data in the region of study is highly relevant, given the scarce number of available in situ sea level observations. Only 4 TGs report data routinely to IOC (http://www.ioc-sealevelmonitoring.org/): Mar del Plata, Puerto Deseado, Puerto Madryn and Ushuaia.

To achieve our objectives, a BPR was deployed near the intersection of J2 tracks 189 and 52 (Fig.1) as part of a project founded by the National Agency for Scientific and Technological Promotion of Argentina. The minimum distance between the coast and the track intersection is 0.9km, and this intersection is one of the few that occurs close to the coast in the PCS. J2, like its predecessors J1 and TOPEX/Poseidon (T/P), is the satellite altimetry mission that has the shortest repeat interval (about 9.9 days). Placing an instrument near a track crossing allows the largest number of data to compare with in situ data for a given period of time. No tidal records have been previously obtained in or near this region.

Bottom pressure was measured by a new calibrated SeaBird SBE26*plus* moored at 30m depth with depth range of 270m; it measures sea level with resolution of 2mm and accuracy of 27mm. The instrument was placed inside a cylindrical tube welded in a vertical position to a train wheel to secure it at the sea bottom. The BPR was placed as near to the bottom as possible to avoid dynamic pressure effects due to high velocity tidal currents [39]. Despite the optimal location to obtain a time series comparable with satellite altimetry data, reaching this region to service the instrument was extremely challenging. Deployment was done with R/V Puerto Deseado on April 1st, 2013. Professional divers performed the mooring recovery and re-deployment twice, by sailing an inflatable semi-rigid boat for two hours between a beach located in the region and the mooring location. We obtained two time series with a total record of 22 months spanning April 2013 to March 2015 (Table I). The BPR was programmed to measure temperature and pressure every two minutes. Pressure measurements were averaged over a 1-minute interval to filter wave effects. The high sampling frequency proved to be a critical factor in properly comparing in situ and altimetry data, given the large tidal range present in the region. The mooring had also separate temperature (*T*) and conductivity (*C*) sensors (SeaBird SBE37, also new). *T* time series obtained from the two instruments were indistinguishable (not shown). After the first two weeks, the conductivity record was useless because of biofouling activity. Two vertical profiles of *C*, *T* and pressure were made at the mooring location using a Seabird SBE911 from R/V Puerto Deseado during deployment in 2013 (early austral autumn) and during the second period of measurement (austral spring). *T* and Salinity (*S*) profiles revealed, in both set of measurements, a very homogeneous water column (not shown), as expected in a shallow region dominated by strong tidal currents. No significant differences were observed between *T* measurements made by SBE911 and SBE26*plus* during the two vertical profiles.

TABLE I
BPR PERIODS OF MEASUREMENTS

Start Date	End Date	Sampling	Number of Measurements
04-01-2013	04-01-2013	2 minutes	155281
12-23-2013	12-23-2013	2 minutes	332679

Both time series are complete, i.e. neither one has missing values.

Based on BPR data, time series of Sea Surface Height (*SSH*) are derived by applying the hydrostatic equation:

$$SSH = \frac{1}{\rho g}(P_{abs} - P_{atm}) \quad \text{(III.1)}$$

where P_{abs} represents the pressure measured by the instrument, P_{atm} atmospheric sea level pressure (*SLP*), g gravity (9.8 m•s^{-2}) and ρ density (kg•m^{-3}). We used daily *SLP* data from the National Center for Environmental Prediction (NCEP) Reanalysis distributed on a global grid of 2.5°x2.5° [19]. During the first deployment (Table I) we measured *SLP* with a 1-hour sampling interval using a meteorological station installed at the park ranger's house in Caleta Los Loros, located 36km from the mooring. No significant differences were found between the in situ *SLP* and the NCEP time series. We thus interpolated the NCEP values to the times of the BPR measurements. Density, ρ, was estimated following the International Thermodynamic Equation of Seawater [18], using *T* and *S* measurements. Because biofouling prevented use of the *S* record, we assumed a constant value of 34, which corresponds to the surface climatological value of the region [16]. ρ was considered constant throughout the water column. This is a reasonable approximation in this region, given the intense mixing generated by tidal currents, as mentioned above.

To obtain in situ *SLA*, the mean sea surface (*MSS*) is extracted from the *SSH*. For in situ data, *MSS* is calculated as the temporal mean of the in situ record. A zoom of the complete time series is displayed in Fig. 3a. It is noticeable that *SLA* varies between ±4m and presents a semidiurnal cycle consistent with the dominant tidal regime of the region.

B. Altimetry Data

The altimetry product used in this study is Sensor Geophysical Data Records (S-GDR) along-track (20Hz) derived from the J2 mission and provided by Archiving, Validation and Interpretation of Oceanographic Data (AVISO, http://www.aviso.altimetry.fr). This dataset has a nominal spatial resolution of about 300m along the tracks, which allows a more detailed analysis of the satellite data accuracy near the coasts than does the traditional averaged 1-Hz dataset (GDR). The S-GDR product contains all the auxiliary data necessary to retrieve the *SSH* and *SLA*: range, altitude, sea state bias, atmospheric (i.e.

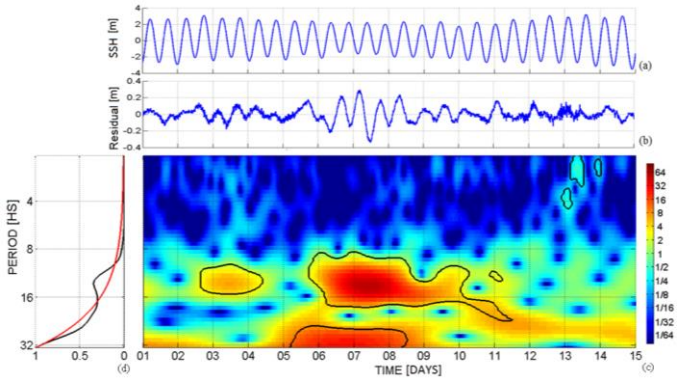

Fig. 3. 15-day segment from 1st to 15th of June 2014 of (a) in situ *SSH* (m) time series, derived from BPR measurements applying (III.1); (b) In situ residual (m) time series; the result of extracting the tidal and storm surge signals from in situ data; and (c) wavelet analysis of the residual; the colorbar represents the power of the wavelet, normalized to have arbitrary units and be comparable to other variables [46]. (d) Global power spectrum (black) of the residual complete time series, and confidence interval (red), it is dimensionless because it is normalized by the variance; period is expressed in hours (hs).

ionosphere, wet and dry troposphere, dynamic atmospheric correction) and ocean (e.g. pole tide, load tide, ocean tide, mean sea surface) corrections. All the information regarding this database can be found in the OSTM/Jason-2 Products Handbook [24]. We analyzed altimetry data along ascending track 189 and descending track 52 in SMG (Fig. 1) for the time period coincident with the in situ record (April 2013 to March 2015).

As mentioned in the previous section, a different retracking is necessary to recover the *SSH* signal near the coast. The retracking method based on the Brown algorithm, which is used to estimate the default range in the J2 S-GDR, fits the waveforms accurately in the open ocean, but it generally fails in coastal regions [47]. In this study we compared the default range with the range estimated from ALES (a retracker capable of retracking both in the open ocean and near the coasts), which showed better performance than standard retrackers in coastal regions, e.g. [27]. The ALES retracker also uses the Brown functional form, but fits only part of the waveform (a sub-waveform), in order to avoid parts of the trailing edge that can be corrupted by bright targets and, at the same time, to guarantee a sufficient fitting quality of the leading edge. A full description is found in [26], and a global coastal dataset containing ALES estimations within 50km of the coastline is can be found at ftp://podaac.jpl.nasa.gov/allData/coastal_alt/L2/ALES/.

C. Tidal Models

In this section we compare the main tidal constituents derived from in situ observations with the values derived from four tidal models, three global and one regional. We also considered the tidal constituents distributed and computed by the Centre of Topography of the Oceans and the Hydrosphere (CTOH, http://ctoh.legos.obs-mip.fr/) closest to the mooring (7km) along the track 189.

To compare models and in situ tidal constants we proceeded as in [34]: we computed the Root Mean Square misfit (RMS_{misfit}) for each tidal constituent selected (III.2) and the Root Sum Square (*RSS*) considering constituents that coincide within all the models analyzed (III.3). The *RSS* allows the comparison among models and therefore the selection of the one that performs best in the study area.

$$RMSmisfit_j = \sqrt{\frac{(H_1\cos(\phi_1)-H_2\cos(\phi_2))^2+(H_1\sin(\phi_1)-H_2\sin(\phi_2))^2}{2}} \quad \text{(III.2)}$$

$$RSS = \sqrt{\frac{\sum_{j=1}^{n} RMS_{misfit_j}{}^2}{n}} \quad \text{(III.3)}$$

where j represents each tidal constituent, H and ϕ are the amplitude and phase. In equation III.2, the sub-indexes 1 and 2 indicate two different datasets, e.g. in situ and a model. In equation III.3, n represents the number of constituents coincident among all data sets considered; in this paper n is 5.

The methodology used to compute the tidal constituents from in situ data and all the tidal models considered are briefly summarized below.

1) Tidal Constituents from In Situ and Satellite Altimetry Data: The least squares method was applied to III.4 to obtain tidal constituents using BPR and satellite data series [23], using the following equation:

$$h(t) = Z_0 + \Delta Z \cdot t + \sum_{j=1}^{n} H_j \cdot f_j \cdot \cos\left((V+u)_j - g_j\right) \quad \text{(III.4)}$$

where $h(t)$ is the height of the tide at observation time t, Z_0 is the mean height of the water level at the beginning of the series, ΔZ is the linear trend of the series, H_j is the amplitude of the j constituent, f_j is the nodal factor of the$j$constituent, $(V+u)_j$ is the value of the equilibrium argument of the j constituent, g_j is the epoch of the j constituent, and n is the number of constituents.

The equilibrium argument and the nodal factors were calculated following [9]. Unlike traditional harmonic analysis [29], [30], [38], (III.4) requires the calculation of both the equilibrium argument and the nodal factor for each observation time, thus avoiding the use of the speed of the constituent. This is because the angular velocity is defined by part *V* of the equilibrium argument and does not consider the temporal variation in part *u* (an 18.61-year period). Considering the long length of the altimetry series, the mean sea level linear variation is taken into account through the first two terms of (III.4).

If data are lacking and/or the sampling interval is variable, it is not possible to apply the Rayleigh criterion to infer the minimum time period required to resolve any two tidal frequency constituents in the harmonic analysis. To decide if the in situ data series could be used to calculate the harmonic constants of the tidal constituents, simulated series were

generated maintaining the intervals between observations. To build the simulated series, harmonic constants from Punta Colorada (provided by SHN, Argentina) were used. The harmonic constants corresponding to all constituents of simulated series were calculated and compared with those obtained from Punta Colorada, obtaining differences smaller than 1mm in amplitude and 0.1° in epoch.

For each amplitude and epoch solved by the harmonic analyses, the uncertainties were calculated using the variance-covariance matrix originated from the least squares equations used for the calculation of the harmonic constituents (Table A1).

2) FES2012: global model based on non-linear barotropic shallow water equations that assimilates both TG and altimetry data. It provides 15 tidal constituents in a 1/8° spatial grid [7].

3) EOT08a: empirical ocean tidal model from multi-mission satellite altimetry. It provides 10 tidal constituents in a spatial grid of 1/8° [36].

4) TPXO8: provides a product especially developed for the Patagonia region that has a spatial resolution of 1/30° [12]. This regional model assimilates T/P, J1, Topex Tandem and ERS satellite data.

IV. Results

A. In situ Tidal Constituents

Following the methodology described in Section III.C, 130 tidal constituents were computed from the 22-month-long in situ time series. Only the 39 constituents with amplitudes that exceeded 1cm are shown (Table A1). The 12 constituents with the largest amplitudes are used in the following sub-section for comparison with tidal models and with the CTOH database. In the PCS, the five constituents with the largest amplitudes that are typically considered by ocean dynamic numerical models are M_2, N_2, S_2, K_1 and O_1 [22], [25], [40], [45]. Results found here show that indeed M_2 is the constituent with the largest amplitude (2.57m) but O_1 is not in the top-five list. Instead, L_2 occupies the fifth place. In order to verify if the tidal constituents computed represent all (or most of) the tide-related signal, we subtracted the tidal signal constructed with the 130 constituents considered from the original time series. The Root mean square (*RMS*) of the residual time series is 0.24m and the *RMS* of the total signal is 1.99m, i.e. the *RMS* of the residual accounts for 12% of the *RMS* of the total signal. Similar residuals were observed from the analysis of three shorter time series in Tierra del Fuego [32]. Close inspection of the residuals shows that at particular times a semidiurnal signal with amplitude of 20cm is present (see an example in Fig. 3b). Using a different method to compute tidal harmonics [11], neither the amplitude nor the location of the semi-diurnal residuals changed. A wavelet analysis confirms that the residual is not permanent (Fig. 3c) but happens often enough to show a significant peak centered at 12.41hs in the time average of the 22 months of the wavelet spectra (Fig. 3d). We attribute this non-permanent signal to non-linear effects. While it is beyond the scope of this paper to investigate what are the processes that generate them, the relatively large contribution to the tidal regime (up to 20cm out of 2.6m, M_2 amplitude) of these residuals deserves attention in future studies.

B. Evaluation of Ocean Tidal Models

Tidal amplitudes and phases from models and the CTOH database were compared to those obtained from in situ data considering the 12 constituents that presented the largest amplitudes in SMG according to the in situ data (Fig. 4 and Table II). Comparing the values provided by different datasets with in situ data, it is noticeable that all of them represent the amplitude better than the phase (Table A2). The determination of tidal phase by global models can be complicated because of the presence of a virtual amphidrome near the region of study. Also, a possible source of error of global models is the lack of L_2 and Nu_2 tidal constituents, whose amplitudes are non-negligible in the Gulf (Fig. 4).

RMS_{misfit} and the *RSS* computed as described in Section 3 are displayed in Table II. Results obtained show that:

- Among global models, EOT08 is the one that better represents the tide in SMG.
- The satellite product from CTOH provides tidal amplitudes and phases along-track for more constituents than presented in this study. The CTOH data were extracted from the nearest point to the mooring along track 189. The comparison with in situ constituents shows this product performs better than global models in this region.
- The best performance among models in SMG is achieved by regional model TPXO8 Atlas.

According to these results, the ocean tidal correction based on the regional model TPXO8is the most suitable for SMG.

We also applied harmonic analysis to along-track satellite altimetry data from T/P, J1 and J2 corresponding to the period October 1992 - July 2016. We considered *SLA* data averaged in space within a radius of 3km from a point located 7km from the mooring location. For this analysis we applied the standard corrections and MLE4 range since ALES retracking is not jet available for the T/P and J1 missions. Results are shown in Table II. This analysis provides the best representation of tides in the region, far better than CTOH and mostly better than TPXO8. Given the results described in section IV.C, we would expect even better results if tidal harmonics were computed with altimetry data retracked by ALES.

C. Impact of ALES Retracking Procedure

In this section we compare ranges obtained with two different retrackers, MLE4 (the standard ocean retracker used in J2 S-GDR) and ALES.

We computed satellite *SSH* as the difference between altitude and range, applying all satellite corrections except the Dynamic

TABLE II

RMS$_{misfit}$ AND *RSS*

Tide Constituent	RMS$_{misfit}$ [cm]				
	Harmonic Analysis of Satellite Altimetry Data	CTOH	Regional Model TPXO8 Atlas	Global Model EOT8a	Global Model FES2012
M_2	3.5	4.8	3.6	10.2	14.5
N_2	0.7	0.8	1.9	1.0	2.8
S_2	0.3	1.8	1.4	4.6	5.6
K_1	1.9	2.0	1.2	1.7	2.4
L_2	1.2	2.0	-	-	-
NU_2	0.2	1.2	-	-	-
K_2	0.8	1.6	0.9	1.9	0.3
LDA_2	0.5	0.3	-	-	-
O_1	0.6	0.7	1.3	1.0	0.5
$2N_2$	1.5	2.0	-	0.5	2.5
P_1	1.8	2.5	1.0	0.3	0.8
Sa	0.8	0.8	-	-	-
	RSS [cm]				
M_2, N_2, S_2, K_1, O_1	4.1	5.7	4.8	11.4	16.0

RMS$_{misfit}$ between the in situ data and each data product, for the 12 selected tidal constituents. *RSS* is calculated considering only the 5 constituents that the 12 selected ones have in common (M_2, N_2, S_2, K_1 and O1).

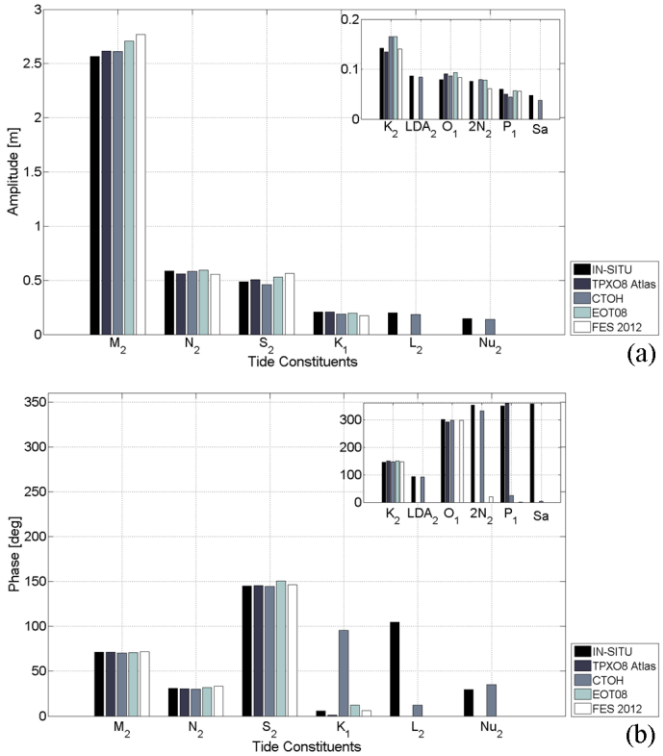

Fig. 4. Tidal amplitude (a) and phase (b) of the 12 selected constituents, estimated by models (TPXO8 Atlas, EOT08, FES2012), and by harmonic analysis of in situ data.

Atmospheric Correction (DAC), the ocean tidal correction and the *MSS*. DAC includes the inverted barometer effect and high frequency variability [6]. We then computed the correlation coefficient between in situ *SSH* and satellite *SSH* as a function of the distance to the coast measured along each track considering the two retrackers (Fig.5). In other words, from each track point we extracted one satellite *SSH* time series that was correlated to in situ *SSH*. Results clearly show the better performance of ALES in the region closer to the coast. For track 52 ALES recovers 80% or more of the data available up to 4km from the coast, while MLE4 drops below 80% of data available at 11km from the coast (Fig. 5b). The correlation coefficient along this track, significant at 95% confidence level (CL), is larger than 0.99 up to 4km for ALES and up to 8.5km for MLE4 (Fig. 5a). For track 189 results show that it is possible to get even closer to the coast. For this track, both ALES and MLE4 recover more than 80% of the data available up to 2km from the coast (Fig. 5d). The correlation coefficient along track 189 is larger than 0.99 up to 1.6km for both retrackers but ALES is more stable along the track (Fig. 5c). Missing waveforms are frequent in the Jason missions at land-to-sea transitions due to failures of the on-board tracker [3], which explains why the loss of data is larger for track 52 than for track 189.

Similar differences between the number of data retrieved from land-to-ocean and ocean-to-land transitions were observed also in the Gulf of Trieste [26] and in the Strait of Gibraltar [13]. Along both tracks, ALES and MLE4 produce indistinguishable results for distances larger than 17km from the coast.

To summarize the impact of ALES, we computed the number of data available in the first 20km closest to the coast for track 52. In that region ALES retrieves 20% more data than MLE4.

D. Impact of Geophysical Corrections

We studied the impact of the geophysical corrections applied to the *SSH* along the two satellite tracks that pass nearby the position of the BPR by computing the correlation between in

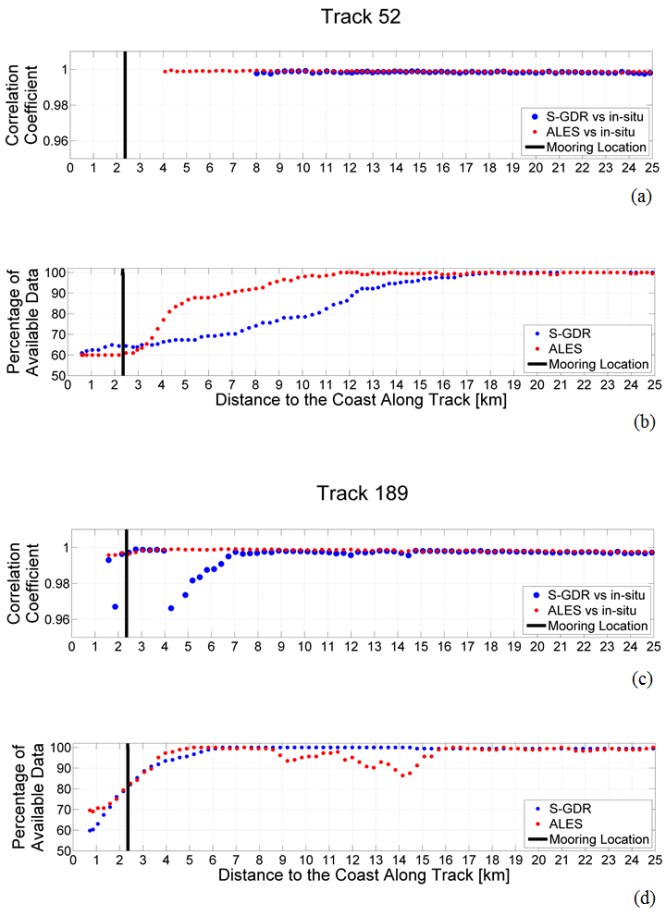

Fig. 5. Correlation coefficient between satellite and in situ *SSH* (a) and percentage of available *SSH* satellite data (b), considering the MLE4 range (blue) and the ALES range (red). (a) and (b) show results for descending track 52, and (c) and (d) for ascending track 189. The black line corresponds to the BPR mooring location. Correlation coefficient was not computed at track points having less than 70% of available data.

situ and satellite time series for each track point. The satellite data has a frequency of 20Hz, which corresponds to one measurement approximately every 300m. Therefore, we assembled time series for each track point as the spatial average of all measurements included in a 300m distance along track, centered in the reference track point. The time series were built for each point of both tracks analyzed, adding satellite corrections one by one. Ocean tide, DAC and *MSS* corrections were also subtracted from the in situ time series when these corrections were applied to satellite data.

The aim of this procedure was to find out how close to the coast satellite data remains valid, and how this data is affected by each satellite correction. Results shown in previous sections were taken into account, therefore the ocean tidal correction used in this section is TPXO8 Atlas and the range considered is ALES.

Results show that the addition of the corrections to the time series helps find high correlation values (95% CL) closer to the coast for both analyzed tracks (Table III). Among all geophysical corrections considered, the ionosphere correction is remarkable as it allows the recovery of data (correlation with in situ data above 0.9) up to 1.5km closer to the coast for track 189 and up to 3.7km for track 52. In addition, another important increase of recovered data is observed when the Solid Earth Tide correction is applied: in particular, for track 189 the distance at which the 0.9 correlation is found reduces from 3.1km to 1.6km (Table III). Finally, when the ocean tidal correction is applied, the closest distance to the coast for which a large correlation is observed increases to 3.1km for track 189, but stays the same (4.1km) for track 52 (Table III).

E. SLA Comparison

In this section we compare in situ *SLA* with the average of satellite *SLA* from both tracks at a distance equal to or less than 3km from the mooring position. Two satellite *SLA* time series were constructed: the first one considers the TPXO8 ocean tidal model and ALES range (see Sections IV.B and IV.C); the second one uses the default configuration provided by AVISO, i.e. ocean tide FES2012 and MLE4 range. In the following we refer to these two time series as "optimal" and "standard", respectively.

When building satellite *SLA* time series, the temporal mean should be as close to zero as possible. However, the mean value of the standard time series is 7.1cm and of the optimal *SLA* is 15.9cm. We attribute this result to the *MSS* model used to correct satellite data [37]. Even though the *MSS* model along the two tracks considered is coherent with the general surface circulation of SMG sketched in Fig. 1 (result not shown), the mean value of the optimal *SLA* time series is far from zero. For this reason, we decided to subtract the temporal mean from the optimal *SLA* time series. Removing the temporal mean from the standard time series decreases the bias from 7.1cm to 4.6cm. In the following we do not remove the temporal mean from the standard time series since our objective is to compare the standard product "as is" with the optimal one.

Fig. 6 and Table IV provide a comparison of the optimal and standard time series with the in situ time series. Optimal time series recovers 70% more data than the standard one (Fig. 6 and Table IV). Moreover, the correlation coefficient between optimal *SLA* and in situ *SLA* is considerably larger than the one obtained with standard *SLA* (0.95 vs. 0.79) (Table IV). The *RMSD* obtained with the optimal time series (12.3cm) is also significantly lower than that obtained with the standard time series (14.1cm). Another way to quantify the differences between the optimal and standard *SLA* time series is through the comparison of the slopes and bias w.r.t. in situ data.

To compute the slopes, we performed a geometric mean regression (GMR) analysis following [21], a method suitable when both the dependent and the independent variables are random. To compute the bias, we calculated the mean value of the difference between satellite and in situ time series.

TABLE III
ANALYSIS OF SATELLITE ALTIMETRY CORRECTIONS

Satellite Corrections applied to altitude - range	Track 052	Track 189
MSS	8.0	4.6
Ionosphere	4.3	3.1
Sea state bias	4.3	3.1
Wet troposphere	4.3	3.1
Dry troposphere	4.3	3.1
Polar tide	4.3	3.1
Loading tide	4.3	3.1
Solid earth tide	4.1	1.6
DAC	4.1	1.6
Ocean tide	4.1	3.1

Closest distance to the coast [km] where correlation between in situ and satellite time series exceeds 0.9. First and second columns show results for data extracted from track 52 and 189, respectively. The corrections were added one by one in the order they appear in the table.

TABLE IV
STATISTICAL ANALYSIS OF SATELLITE *SLA* TIME SERIES

	Standard *SLA*	Optimal *SLA*
Correlation Coefficient	0.79	0.95
RMSD (cm)	14.1	12.3
GMR slope	1.14	0.99
Bias (cm)	7.1	3.5

Statistical analysis between satellite time series and in situ measurements. Both correlation values are significant (95%CL), even though the standard time series is composed of only nine values.

Results (Table IV) show that the optimal *SLA* time series has a lower bias and a slope that is closer to 1 than the standard *SLA* time series. Thus, a significant improvement is obtained with the optimal *SLA* time series due to the retracking algorithm (ALES) and to the regional tidal model (TPXO8) considered. In other words, results demonstrate that it is possible to (i) increase the amount of available data of the along-track altimetry *SLA* in coastal areas and (ii) to improve its accuracy by selecting the ALES retracking algorithm and an accurate tidal model.

V. DISCUSSION AND CONCLUDING REMARKS

In this paper we compared 20-Hz S-GDR Jason-2 satellite altimetry data obtained from the crossing tracks 52 and 189 in San Matias Gulf, Argentina, with a 22-month-long time series of sea level obtained by a bottom pressure recorder deployed 1.3km from the nominal intersection of the two tracks and 2.2km from the coast. Results show that there are two factors that largely affect satellite altimetry data near the coasts of San Matias Gulf: the retracking algorithm and the ocean tidal correction used.

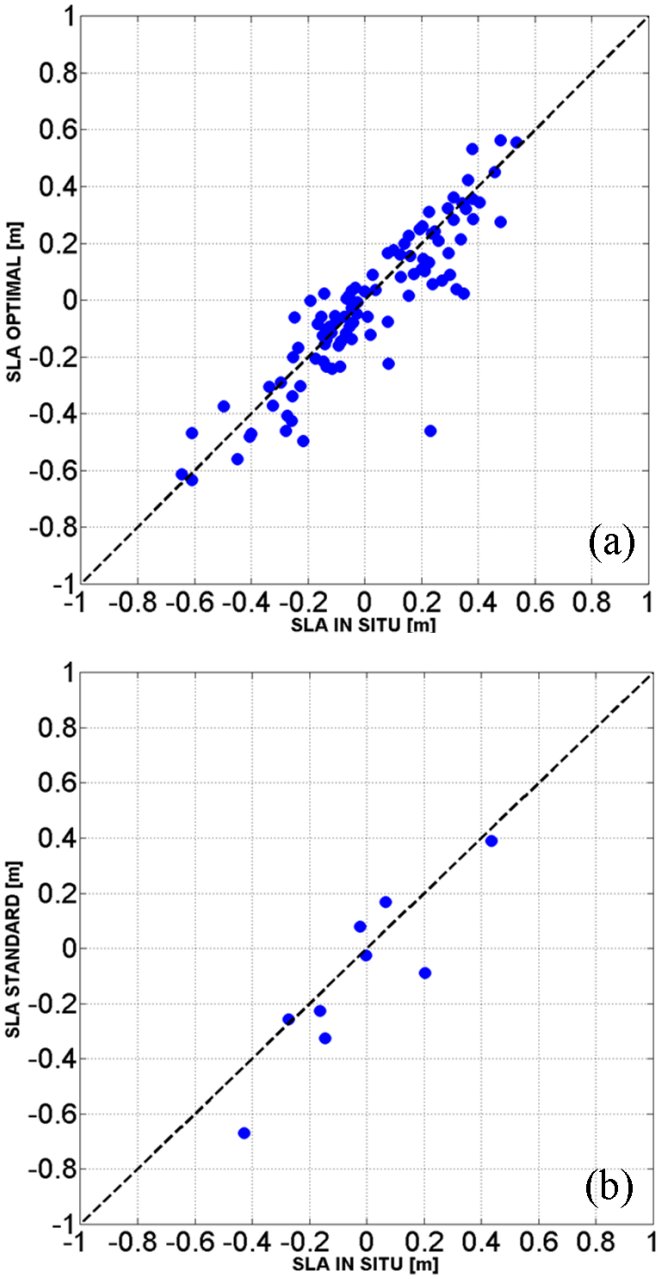

Fig. 6. (a) Scatter plot between the *SLA* constructed using ALES range, the TPXO8 Atlas ocean tidal model correction and Dynamic Atmospheric Correction (DAC) and the *SLA* obtained from in situ measurements. (b) Scatter plot between the *SLA* constructed using the standard corrections and the *SLA* based on in situ measurements. In both figures, the dashed line represents a perfect fit.

The retracking method selected was critical to recover more useful data closer to the coast. We compared two retracking algorithms: MLE4, the standard method for the open ocean based on the Brown model, and ALES, an algorithm specially developed for both the open ocean and coastal areas. Results show that ALES is able to recover more and better data near the coast than the Brown model, in particular for the track with a

land-to-ocean transition. For this track, correlation between in situ and altimetry data is larger than 0.99 (95%CL) up to 1.6km from the coast when altimetry data are retracked with ALES. Using MLE4, data availability stops 8.5km from the coast.

The ocean tidal correction has a large impact in the estimation of sea level anomaly in San Matias Gulf due to the macrotidal regime present there. The error in the estimation of tides can be attributed to two different causes: 1) the presence of an intermittent semi-diurnal signal (*RMS* 24cm) that cannot be represented by the linear combination of tidal constituents and therefore still remains unpredictable; 2) the absence of certain constituents in tidal models that present large amplitudes in SMG. Results show that among the tidal models considered, the regional model TPXO8 was the one that better represents the tidal regime in the region (*RSS* of 4.8cm). This result is consistent with previous studies carried out in several macrotidal regions, e.g. [43], [34]. However, the best representation of tides in SMG was obtained by harmonic analyses of a 23 year 1-Hz satellite data time series constructed considering data with standard corrections and range from TOPEX/Poseidon, Jason-1 and Jason-2 satellite missions (*RSS* 4.1cm). According to the results presented, when TOPEX/Poseidon and Jason-1 data retracked by ALES becomes available, we would expect even lower *RSS* values.

Results highlight the quality of the satellite altimetry data even very close to the coast. As long as the coastal altimetry community continues to improve corrections and retracking techniques, we can expect that satellite altimetry data will become more and more reliable closer to the coast. Another essential ingredient to achieve improvements in coastal altimetry is the availability of long-term in situ tide gauge time series of good quality. When the tidal amplitude is large, the time sampling interval of in situ data is a key factor. If a traditional 1-hour sample interval were considered in our analysis, instead of the 2-minute interval selected for this study, *RSS* and correlation between altimetry and in situ data would decrease by 7.8% and 1%, respectively.

Finally, in situ data also highlighted our limited knowledge of the retrieval of tides in complex areas like the SMG. Further studies are required to comprehend the generation mechanism of the non-permanent semi-diurnal signal found in the in situ time series. If we succeed in the understanding and prediction of this signal, it will be possible to extract it from satellite altimetry data, and hence obtain a more accurate sea level product in coastal regions.

APPENDIX

TABLE A1
IN SITU TIDAL AMPLITUDE AND PHASE

	Tidal Constituent	Velocity [°/h]	Amplitude [cm]	Amplitude Error [cm]	Phase [°]	Phase Error [º]
1	M_2	28.98410424	256.58	0.05	71.35	0.01
2	N_2	28.43972954	58.73	0.05	30.85	0.05
3	S_2	30	48.54	0.05	145.16	0.06
4	K_1	15.04106864	20.69	0.06	5.91	0.15
5	L_2	29.52847893	20.19	0.06	104.66	0.17
6	Nu_2	28.51258317	14.80	0.05	29.54	0.19
7	K_2	30.08213728	14.26	0.06	145.33	0.25
8	LDA_2	29.4556253	8.68	0.05	93.96	0.33
9	O_1	13.9430356	7.88	0.06	301.73	0.42
10	$2N_2$	27.89535485	7.56	0.05	352.67	0.39
11	L_2a	29.5377626	6.87	0.07	275.84	0.59
12	P_1	14.95893136	6.02	0.05	349.56	0.47
13	Mf	1.098033041	5.33	0.07	163.96	0.77
14	Sa	0.041066678	4.75	0.05	357.14	0.69
15	Msn_2	30.5443747	4.13	0.05	19.16	0.64
16	Ssa	0.082137279	3.89	0.05	171.16	0.73
17	Mo_3	42.92713984	3.71	0.06	316.09	0.87
18	Mu_2	27.96820847	3.59	0.05	140.45	0.76
19	Mk_3	44.02517288	3.25	0.05	34.29	0.94
20	T_2	29.95893332	3.16	0.05	149.69	0.89
21	M_4	57.96820847	3.08	0.05	74.93	0.86
22	Msf	1.015895763	2.47	0.04	93.38	1.02
23	S_1	15	2.47	0.05	113.12	1.15
24	$2Sm_2$	31.01589576	2.45	0.05	50.46	1.11
25	Mks_2	29.06624152	2.25	0.06	142.09	1.57
26	Ta_1	27.89071301	1.99	0.05	230.44	1.49
27	So_3	43.9430356	1.87	0.06	21.25	1.79
28	Oq_2	27.3416964	1.59	0.07	263.69	2.49
29	M_6	86.95231271	1.52	0.04	16.42	1.68
30	Mns_2	27.42383378	1.52	0.05	141.05	1.75
31	Skm_2	31.09803304	1.48	0.06	74.37	2.36
32	M_3	43.47615636	1.42	0.05	149.70	1.88
33	No_3	42.38276514	1.38	0.06	268.08	2.34
34	Kj_2	30.62651197	1.35	0.07	213.48	3.01
35	Mn_4	57.42383378	1.35	0.05	31.37	1.96
36	Sk_3	45.04106864	1.28	0.06	53.57	2.46
37	Mnk_2S_2	27.50597106	1.23	0.06	3.30	2.76
38	$2Nk_2S_2$	26.96159636	1.17	0.06	179.47	2.89
39	Mm	0.544374696	1.04	0.04	31.24	2.42

Tidal amplitude and phase for the 39 constituents whose amplitudes exceed 1cm, and the corresponding uncertainties. They result from applying harmonic analysis to in situ data.

In order to verify if tidal models and the CTOH tidal product represent better the tidal amplitude than the phase, we calculated the *NRMSD* (A.1) between in situ and modeled values, normalized by the range of the variable considered. It is evident from the results obtained (Table A2) that all databases considered represent better the tidal amplitudes than the tidal phases.

$$\mathrm{NRMSD} = \frac{\sqrt{\frac{\sum_{i=0}^{n}(Y_{\mathrm{model}} - Y_{\mathrm{in\ situ}})}{n}}}{\max(Y_{\mathrm{in\ situ}}) - \min(Y_{\mathrm{in\ situ}})} \quad \text{(A.1)}$$

TABLE A2
NRMSD BETWEEN IN SITU AND ESTIMATED TIDAL AMPLITUDE AND PHASE

NRMSD	Tidal Amplitudes	Tidal Phases
TPXO8	0.007	0.419
FES2012	0.026	0.397
EOT8a	0.017	0.509
CTOH	0.008	0.409

Where Y can be either the tidal amplitude or the phase; *n* is the number of tidal constituents considered. In this case we used the 5 constituents present in all databases analyzed.

AKNOWLEDGEMENTS

Support was provided through the following grants:
MINCYT-ECOS-Sud, Corrientes del Atlántico Sudoeste a partir de datos in situ y de altimetría, A14U02, PI: M. Saraceno, 2015-2017.
CONICET-YPF, El rol de la corriente de Malvinas en la dinámica de la plataforma continental patagónica, PIO 13320130100242, PI: M. Saraceno, $ ARG 641.667, 2014-2016.
EUMETSAT/CNES (France), Southwestern Atlantic currents from in situ and satellite altimetry data, DSP/OT/12-2118, PI: M. Saraceno, euro 233,475, 2013-2016.

REFERENCES

[1] Andersen, O. B. and Scharroo, R. "Range and Geophysical Corrections in Coastal Regions: And Implications for Mean Sea Surface Determination", in *Coastal Altimetry*, edited by S. Vignudelli, A. G. Kostianoy, P. Cipollini, and J. Benveniste, Berlin: Springer, 2011, pp103–145.

[2] Beier, E. J. and Akaprahamyan, R. (1991). Variación estacional de la circulación inducida por el viento en el Golfo San Matías aplicando el modelo Cox/CIMA. Presented at IV Jornadas Nacionales de Ciencias del Mar. Madryn, Argentina.

[3] Brooks, R. L., Lockwood, D. W., Lee, J. E., Handcock, D. and Hayne, G. S., "Land effects on TOPEX radar altimeter measurements in Pacific Rim coastal zones", in *Remote sensing of the Pacific by satellites*, R. A. Brown (Ed.), 1998, pp 175–198.

[4] Brown, G. (1977). The average impulse response of a rough surface and its applications. IEEE Transactions on antennas and Propagation, 25(1), 67-74.

[5] Burrage, D. M., Steinberg, C. R., Mason, L. B., & Bode, L. (2003). Tidal corrections for TOPEX altimetry in the Coral Sea and Great Barrier Reef Lagoon: Comparisons with long-term tide gauge records. *Journal of Geophysical Research: Oceans*, *108*(C7).

[6] Carrère, L., Lyard, F. (2003). Modeling the barotropic response of the global ocean to atmospheric wind and pressure forcing – comparisons with observations. *Geophys Res Lett. 30(6)*.1275.doi:10.1029/2002GL016473.

[7] Carrère, L., Lyard, F., Cancet, M., Guillot, A. and Roblou, L. (2012). FES2012: A new global tidal model taking advantage of nearly 20 years of altimetry. Presented at proceedings of meeting "20 Years of Altimetry", Venice, Italy.

[8] Carreto, J. I., Casal, A. B., Hinojal, A., Laborde, M. A. and Verona, C. A. (1974). Fitoplancton, pigmentos y condiciones ecológicas del Golfo San Matías. Informe no. 10. *Com. de Invest. Cient., La Plata*.

[9] Cartwright, D. E.(1985). Tidal prediction and modern time scales. *Int. Hydrographic Rev.* LXII (1), pp 127-138.

[10] Cipollini, P., Benveniste, J., Bouffard, J., Emery, W., Fenoglio-Marc, L., Gommenginger, C. and Mercier, F. (2010). The role of altimetry in coastal observing systems. *Proceedings of Ocean Obs, 9*, pp 181-191.

[11] Codiga, D. L. (2011). Unified tidal analysis and prediction using the UTide Matlab functions. Narragansett, RI: Graduate School of Oceanography, University of Rhode Island.

[12] Egbert, G. D. and Erofeeva, S. Y. (2002). Efficient inverse modeling of barotropic ocean tides. *Journal of Atmospheric and Oceanic Technology*. 19(2), pp 183-204.

[13] Gómez-Enri, J., Cipollini P., Passaro, M., Vignudelli, S., Tejedor, B. and Coca, J. (2016). Coastal Altimetry Products in the Strait of Gibraltar.

[14] Gommenginger, C., Thibaut, P., Fenoglio-Marc, L., Quartly, G., Deng, X., Gómez-Enri, J., Challenor, P. and Gao, Y. (2011). "Retracking altimeter waveforms near the coasts", in Coastal altimetry. Springer Berlin Heidelberg, pp. 61-101.

[15] González, R. A., Narvarte, M. A. and Caille, G. M. (2007). An assessment of the sustainability of the hake Merluccius hubbsi artisanal fishery in San Matías Gulf, Patagonia, Argentina. *Fisheries Research*. *87*(1), pp58-67.

[16] Guerrero, R. A., and Piola, A. R. (1997). Water masses in the continental shelf. *The Argentine sea and its fisheries resources*, *1*, pp107-118.

[17] Idris, N. H., Deng, X. and Andersen, O. B. (2014). The importance of coastal altimetry retracking and detiding: a case study around the Great Barrier Reef, Australia. *International Journal of Remote Sensing*. *35*(5), pp1729-1740.

[18] IOC, SCOR and IAPSO, 2010: The international thermodynamic equation of seawater - 2010: Calculation and use of thermodynamic properties. Intergovernmental Oceanographic Commission, Manuals and Guides No. 56, UNESCO (English), pp196. Available from http://www.TEOS-10.org.

[19] Kalnay, E., Kanamitsu, M., Kistler, R., Collins, W., Deaven, D., Gandin, L. and Zhu, Y. (1996). The NCEP/NCAR 40-year reanalysis project. *Bulletin of the American Meteorological Society*. 77(3), pp 437-471.

[20] Laiz, I., Gómez-Enri, J., Tejedor, B., Aboitiz, A. and Villares, P. (2013). Seasonal sea level variations in the gulf of Cadiz continental shelf from in situ measurements and satellite altimetry. *Continental Shelf Research*. *53*, pp 77-88.

[21] Leng, L., Zhang, T., Kleinman, L., and Zhu, W. (2007). Ordinary least square regression, orthogonal regression, geometric mean regression and their applications in aerosol science. In *Journal of Physics: Conference Series* (Vol. 78, No. 1, p. 012084). IOP Publishing.

[22] Moreira, D., Simionato, C. G. and Dragani, W. (2011). Modeling ocean tides and their energetics in the North Patagonia Gulfs of Argentina. *Journal of Coastal Research. 27*(1), pp 87-102.

[23] Oreiro, F. A., D'Onofrio, E. E., Grismeyer, W. H., Fiore, M. M. E. and Saraceno, M. (2014). Comparison of tide model outputs for the northern region of the Antarctic Peninsula using satellite altimeters and tide gauge data. *Polar Science*. 8, pp10-23.

[24] OSTM/Jason-2 products handbook (2015). CNES: SALP-MU-M-OP-15815-CN, EUMETSAT: EUM/OPS-JAS/MAN/08/0041, JPL: OSTM-29-1237, NOAA/NESDIS: Polar Series/OSTM J, 400(1).

[25] Palma, E. D., Matano, R. P. and Piola, A. R. (2004). A numerical study of the Southwestern Atlantic Shelf circulation: Barotropic response to tidal and wind forcing. *Journal of Geophysical Research: Oceans*, *109*(C8).

[26] Passaro, M., Cipollini, P., Vignudelli, S., Quartly, G. D. and Snaith, H. M. (2014). ALES: A multi-mission adaptive Subwaveform retracker for coastal and open ocean altimetry. *Remote Sensing of Environment*. *145*, pp173-189.

[27] Passaro, M., Cipollini, P., and Benveniste, J. (2015). Annual sea level variability of the coastal ocean: The Baltic Sea - North Sea transition zone. *Journal of Geophysical Research: Oceans*. *120*(4), pp 3061-3078.

[28] Piola, A. R., and Scasso, L. M. (1988). Circulación en el golfo San Matías. *Geoacta*. *15* (1), pp 33-51.

[29] Pugh, D. T. (1987). Tides, Surges and Mean Sea-Level. John Wiley and Sons Ltd., Chichester.

[30] Pugh, D. T. (2004). Changing Sea Levels: Effects of Tides, Weather and Climate. Cambridge University Press, U.K.

[31] Puissant, A., Lefevre, S., and Weber, J. (2008). Coastline extraction in VHR imagery using mathematical morphology with spatial and spectral knowledge. In SPRS Congress Beijing 2008, pp. 1305-1310.

[32] Richter, A., Mendoza, L., Perdomo, R., Hormaechea, J. L., Savcenko, R., Bosch, W., & Dietrich, R. (2012). Pressure tide gauge records from the Atlantic shelf off Tierra del Fuego, southernmost South America. Continental Shelf Research, 42, 20-29.

[33] Ruiz Etcheverry, L. A., M. Saraceno, A. R. Piola, G. Valladeau, and Moller, O. O. (2015), A comparison of the annual cycle of sea level in coastal areas from gridded satellite altimetry and tide gauges, *Cont. Shelf Res.*. 92, pp87–97.

[34] Saraceno, M., D'Onofrio, E. E., Fiore, M. E. E., and Grismeyer, W. H. (2010). Tide model comparison over the Southwestern Atlantic Shelf. *Continental Shelf Research*. *30*(17),pp 1865-1875.

[35] Saraceno, M., Simionato, C. G., and Ruiz-Etcheverry, L. A. (2014). Sea surface height trend and variability at seasonal and interannual time scales in the Southeastern South American continental shelf between 27° S and 40° S. *Continental Shelf Research*. *91*, pp 82-94.

[36] Savcenko, R. and Bosch, W. (2008). EOT08a-a new global ocean tide model derived by empirical analysis of multi-mission altimetry data. *Geophys. Res. Abst*., 10, EGU2008-A, 7470.

[37] Schaeffer, P., Faugere, Y., Legeais, J. F., Ollivier, A., Guinle, T., and Picot, N. (2012). The CNES_CLS11 global mean sea surface computed from 16 years of satellite altimeter data. *Marine Geodesy*, *35*(sup1), 3-19.

[38] Schureman, P. (1988). Manual of Harmonic Analysis and Prediction of Tides. *U.S. Department of Commerce, Coast and Geodetic Survey*. Special Publication No. 98.

[39] Shih, H. and Baer, L. (1991). "Some Errors in Tide Measurement Caused by Dynamic Environment." in Tidal Hydrodynamics, edited by B. B. Parker, pp 641-671. John Wiley and Sons.

[40] Simionato, C. G., Dragani, W., Nuñez, M. and Engel., M. "A set of 3-D nested models for tidal propagation from the argentinean continental shelf to the Río de la Plata estuary-Part I. M2." *Journal of Coastal Research*. 2004, pp 893-912.

[41] Stammer, D., Ray, R. D., Andersen, O. B., Arbic, B. K., Bosch, W., Carrère, L.,Cheng, Y., Chinn, D. S., Dushaw, B. D., Egbert, G. D., Erofeeva, S. Y., Fok, H. S., Green, J. A. M., Griffiths, S., King, M. A., Lapin, V., Lemoine, F. G., Luthcke, S. B., Lyard, F., Morison, J., Müller, M., Padman, L., Richman, J. G., Shriver, J. F., Shum, C. K., Taguchi, E., Yi, Y. (2014). Accuracy assessment of global barotropic ocean tide models. Reviews of Geophysics, 52(3), 243-282.

[42] Strub, P. T., James, C., Combes, V., Matano R. P., Piola, A. R., Palma, E. D., Saraceno, M., Guerrero, R. A., Fenco, H. and Ruiz- Etcheverry, L. A. (2015), Altimeter-derived seasonal circulation on the southwest Atlantic shelf: 27°S–43°S, J. *Geophys. Res. Oceans.* 120, pp 3391–3418, doi:10.1002/2015JC010769.

[43] Testut, L., and Unnikrishnan, A. S. (2016). Improving modeling of tides on the continental shelf off the west coast of India. Journal of Coastal Research, 32(1), 105-115.

[44] Thomson, R. E., and Emery, W. J. (2014). Data analysis methods in physical oceanography. Newnes.

[45] Tonini, M. H., Palma, E. D. and Piola, A. R. (2013). A numerical study of gyres, thermal fronts and seasonal circulation in austral semi-enclosed gulfs. *Continental Shelf Research*. *65*, pp97-110.

[46] Torrence, C. and Compo, G. P. (1998). A practical guide to wavelet analysis. *Bulletin of the American Meteorological society*. *79*(1),pp 61-78.

[47] Vignudelli, S., Cipollini, P., Roblou, L., Lyard, F., Gasparini, G. P., Manzella, G. and Astraldi, M. (2005). Improved satellite altimetry in coastal systems: Case study of the Corsica Channel (Mediterranean Sea). *Geophysical Research Letters*. *32*(7).

[48] Vignudelli, S., Kostianoy, A. G., Cipollini, P., and Benveniste, J. (Eds.). (2011). *Coastal altimetry*. Springer Science & Business Media.

[49] Williams, G., Sapoznik, M., Ocampo-Reinaldo, M., Solis, M., Narvarte, M., González, R. and Gagliardini, D. (2010). Comparison of AVHRR and SeaWiFS imagery with fishing activity and in situ data in San Matías Gulf, Argentina. *International Journal of Remote Sensing*. 31 (17-18), pp 4531-4542.